

Article

Influence of Varying the Spraying Distance on the Structural-Phase State and Mechanotribological Properties of 86WC-10Co-4Cr-Based Coatings Obtained by the HVOF Method

Bauyrzhan Rakhadilov¹, Nazerke Muktanova^{2,3,*} , Daur Kakimzhanov^{2,3} , Meruert Adilkanova², Sherzod Kurbanbekov⁴ and Saule Abdulina²

¹ Research Center “Surface Engineering and Tribology”, Sarsen Amanzholov East Kazakhstan University, Ust-Kamenogorsk 070000, Kazakhstan; rakhadilov@mail.ru

² International School of Engineering, Daulet Serikbaev East Kazakhstan Technical University, Ust-Kamenogorsk 070002, Kazakhstan; daur_97@mail.ru (D.K.); milka160281@mail.ru (M.A.); abdulina.saule@mail.ru (S.A.)

³ PlasmaScience LLP, Ust-Kamenogorsk 070010, Kazakhstan

⁴ Department of Physics, Khoja Akhmet Yassawi International Kazakh-Turkish University, Turkestan 161200, Kazakhstan; sherzod05.88@gmail.com

* Correspondence: muktanovan@gmail.com

Abstract: This paper presents the results of a metallographic and tribological study of 86WC-10Co-4Cr coatings obtained by the HVOF method on the Termika-3 unit at varying spraying distances. The influence of spraying distance on the coating microstructure, phase composition, as well as mechanical and tribological properties, was studied. According to the results of the study, it was found that the optimum spraying distance for 86WC-10Co-4Cr coatings with improved wear resistance and hardness characteristics and low porosity is 300 mm.

Keywords: wear resistance; metallo-ceramic coating; microstructure; phase composition



Citation: Rakhadilov, B.; Muktanova, N.; Kakimzhanov, D.; Adilkanova, M.; Kurbanbekov, S.; Abdulina, S.

Influence of Varying the Spraying Distance on the Structural-Phase State and Mechanotribological Properties of 86WC-10Co-4Cr-Based Coatings Obtained by the HVOF Method. *Coatings* **2024**, *14*, 264. <https://doi.org/10.3390/coatings14030264>

Academic Editor: Hideyuki Murakami

Received: 5 February 2024
Revised: 16 February 2024
Accepted: 19 February 2024
Published: 22 February 2024



Copyright: © 2024 by the authors. Licensee MDPI, Basel, Switzerland. This article is an open access article distributed under the terms and conditions of the Creative Commons Attribution (CC BY) license (<https://creativecommons.org/licenses/by/4.0/>).

1. Introduction

One of the main technical tasks of oil and oil product transportation is the creation of a highly organized system of pipeline transport communications, providing high reliability and complete environmental safety. This can be provided by the creation and manufacturing of high-quality pipeline valves and other elements of the pipeline transportation system using high-strength and wear-resistant materials.

In the Republic of Kazakhstan, large plants include the joint stock company “Ust-Kamenogorsk Armature Plant” (Ust-Kamenogorsk), the limited liability partnership “Kazakhstan Armature Plant” (Temirtau), the joint stock company “Ust-Kamenogorsk Industrial Armature Plant” (Ust-Kamenogorsk), the limited liability partnership “Pavlodar Pipeline Armature Plant” (Pavlodar), and the Atyrau Pipeline Armature Plant (Atyrau). Consumers of pipeline valves produced in the Republic of Kazakhstan, including gate valves (gate, wedge, and check valves), are the largest energy producing, oil refining, and metallurgical enterprises of the Republic of Kazakhstan and the Commonwealth of Independent States [1].

One of the technical tasks of the above-mentioned plants is to improve the reliability and durability of gate valves. Gate valves are one of the most important elements in the transportation of oil and gas and in the process of production from the well and are utilized in a complex network of pipelines, determining the conditions of safe operation and environmental protection.

The intensification of production and increasing the competitiveness of domestic products requires the use of modern materials with improved physical and chemical properties. However, domestic plants producing pipeline valves, namely gate valves, still

use traditional and outdated surfacing and coating technologies, which do not provide good tribological and corrosion characteristics for the seat gate unit.

For example, the Ust-Kamenogorsk Valve Plant applies the technology of electric arc cladding with the dispersion-hardening steel and 10X17H8C5Γ2T-type of sealing surfaces of gates of heavy-welded oil pipeline valves. However, this method does not provide the surface with good mechanical and tribological characteristics. Therefore, in the conditions of the Ust-Kamenogorsk armature plant, for an increase in the wear-resistance of cladding materials, an 10X17H8C5Γ2T ultrasonic hardening/finishing treatment is applied, which simultaneously increases the surface hardness of the clad metal and the surface roughness and creates an antifriction surface layer. Nevertheless, this combined technology does not ensure the service life of gate valves at the same level as imported ones and is not economically feasible. Therefore, this plant is now widely used to improve the service life of gate valves using galvanic chrome-plating technology, which is environmentally harmful. In developed countries today, there are strict restrictions on processes that use hexavalent chromium emissions [2].

Other plants in Kazakhstan still have not developed and implemented cladding or spraying technologies in the production of gate valve parts. For example, the JSC “Ust-Kamenogorsk plant of industrial valves” produces small-size gate valves without the use of a surface treatment (surfacing or spraying), which makes them less competitive compared to imported products [3]. Thus, in our opinion, to increase the competitiveness of domestic gate valves used in the oil production industry and to ensure import substitution, it is necessary to develop and introduce the modern gas–thermal technologies of protective coating applications. In addition, it is necessary to replace the technology of galvanic chrome plating with gas–thermal technologies. In industrialized countries, the mastering of gas–thermal spraying techniques is taking place by replacing “dirty” galvanic technologies.

As is known from the works of S.S. Poloskov [4], S.A. Tukov, M.V. Korchagin, and S.O. Kireev [5], during operation, the components of valves used in the oil industry are subjected to intensive erosion, corrosion, and wear, which leads to a sharp decrease in their durability. The erosion and corrosion of gate valves used in the oil industry is a serious problem. This is because suspended sand particles in the oil and gas flow cause the erosion of certain critical components such as gate valves and seat rings, resulting in significant operating costs. On the other hand, the corrosion of these components due to chlorides, sulfides, and other impurities in the crude oil and gas can also lead to leaks and premature failures. To counter the combination of friction and wear, various coatings and surface treatments are used on gates and seats. These include hard chrome plating, electrolytic nickel plating, conversion coatings, diffusion treatments, thermal spray coatings, and weld surfacing. Of these, thermal spraying is one of the most effective methods in terms of world practice and a modern analogue of the above methods [6].

According to sources [7–9], various thermal spraying methods such as air plasma spraying (APS), vacuum plasma spraying (VPS), detonation guns, arc spraying, flame spraying, and high velocity oxygen–fuel (gas–flame) spraying (HVOF) are used in ceramic–metal composite (cermets) coatings, particularly tungsten–tungsten–cobalt–carbide (WC-Co), tungsten–cobalt–cobalt–carbide–chromium (WC-Co-Cr), and chromium–carbide–nickel–chromium (Cr₃C₂-NiCr) [10–13].

The advantage of these materials is their high resistance to abrasion, erosion, and cavitation wear, and the ceramic coatings obtained from them are characterized by increased hardness, low thermal conductivity coefficients, high corrosion and oxidation resistance, and high resistance to abrasion and erosion [14–16].

Carbide–cobalt (WC-Co) composites have proven themselves as wear- and erosion-resistant coatings in many industries, for instance, in the aerospace and marine sectors (aircraft landing gear, propellers, gas turbines, hydraulic drives), oil and gas drilling, metal cutting, mining, metal forming, the pulp and paper industry, geothermal energy, power generation (gas turbines), and marine structures [17–23].

As an improvement of the traditional WC-Co powder, WC-Co-Cr powder is being increasingly used in industry because of the superior wear resistance and corrosion resistance of this composition [16,21,24]. Cr acts as the most basic element of corrosion resistance [25,26]. The higher wear characteristics are explained by the fact that the CoCr matrix provides better binding to carbides and therefore prevents the loss of carbides at the spray particle boundaries during wear [27].

WC-Co-Cr coatings can be applied using various spray techniques such as air plasma spraying (APS), vacuum plasma spraying (VPS), detonation guns, arc spraying, flame spraying, and high velocity oxygen–fuel spraying (HVOF) [28–30]. However, the HVOF process has been recognized for its various advantages, including lower porosity, reduced decomposition reactions, higher tungsten carbide (WC) retention, and better adhesion between tungsten carbide (WC) and the metal bonding phase [31–37].

In [38], a comparative study of WC-10Co-4Cr and WC-Co coatings sprayed using the HVOF method was carried out in terms of performance under dry abrasive wear conditions at room temperature at a load of 10 N. WC-Co-Cr resulted in 20 times less wear by volume of material removed compared to WC-Co, as a function of the number of wear cycles. The WC-Co-Cr coating has its wear properties due to the high volume fraction of hard and tough WC grains in the Co-based metallic binder phase. The presence of a metallic binder provides a certain degree of coating strength compared to pure ceramic tile, but the binder becomes brittle if large amounts of W and C are dissolved in it during spraying [39]. The performance of WC-based coatings is also highly dependent on the composition and structure of the initial powders. Recent studies have shown that the wear resistance and corrosion performance of HVOF carbide (cermet) coatings can be improved if the carbide particle size is reduced to a submicron scale or nanoscale [40–43]. These works indicated that the decomposition and decarburization of carbide particles are responsible for phase transformations and affect the properties of WC-Co-based coatings.

Thus, the careful optimization of spray parameters and the selection of raw powder materials are necessary to ensure sufficient particle velocity to produce a viable coating, while preventing the overheating of the particles to prevent decarburization.

WC-Co-Cr coatings were chosen as a good potential material for this application because this material exhibits wear resistance comparable to the commonly used WC-Co but also offers improved corrosion resistance.

In addition, the coatings selected for gates and seats must respond to stringent operational requirements and provide a reliable gas-tight metal-to-metal seal. A literature review has shown that the coating process using high velocity oxygen-fuel spraying (HVOF) improves surface properties, increasing wear resistance and corrosion resistance, and provides an effective seal between functional surfaces. However, the regularities of the formation of structural-phase states of HVOF coatings WC-Co-Cr and their influence on tribological properties have been insufficiently studied. Therefore, a complex experimental study of tungsten carbide-based coatings' structural-phase content depending on the technological spraying mode was necessary.

Thus, the aim of this paper was to investigate the structural-phase state and mechanical-tribological properties of 86WC-10Co-4Cr-based coatings prepared by HVOF method.

All the research of the authors related to the HVOF technology were performed on through PlasmaScience LLP (Ust-Kamenogorsk, Kazakhstan) [44].

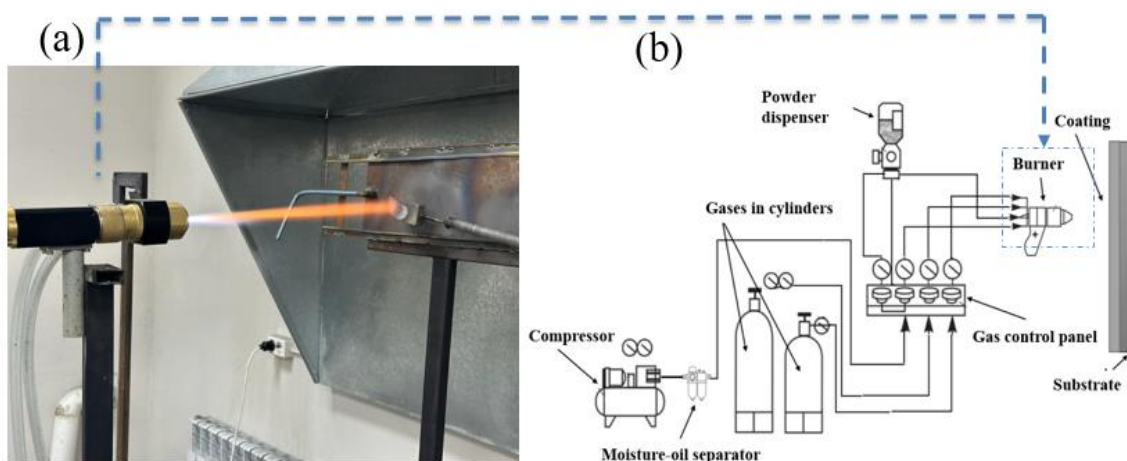
2. Materials and Methods

In the present work, in order to provide an improvement of the tribological properties of the “gate-seat” assembly of the valve of pipeline valves, the sintered metal–ceramic powder of tungsten carbide in a cobalt–chromium matrix 86WC-10Co-4Cr (JSC “Polema”, Tula, Russia) with a particle size of $15 \div 50$ microns was used. As a substrate, samples from high-alloy, corrosion-resistant 30Cr13 steel (AISI 420S) with thickness of 4 mm were used (used in the construction of the gate assembly). The chemical composition of the substrate and 86WC-10Co-4Cr coating materials is presented in Table 1.

Table 1. Chemical composition of base material and coatings (wt.%).

Substrate material 30Cr13 steel (AISI 420S)												
C	Si	Mn	P	S	Cr	Mo	Ni	V	Ti	Cu	W	Fe
0.26–0.35	<0.8	<0.8	<0.03	<0.025	12–14	<0.3	<0.6	<0.2	<0.2	<0.3	<0.2	rest
Coating 86WC-10Co-4Cr												
C	Co	Cr	Fe	W	Other							
5.34	9.86	4.03	0.08	Basis	<0.3							

The variable parameter was the spraying distance: L1-100 mm, L2-200 mm, and L3-300 mm. Before spraying, the substrate surface was degreased and sandblasted at a pressure of 0.6 MPa using electrocorundum. The HVOF Termika-3 high-velocity oxygen fuel spraying unit (manufactured by Plasmacentr LLC, St. Petersburg, Russia) was used for the coating [45]. The HVOF Termika-3 unit operates based on a process that utilizes gas combustion to create thermal energy. This energy is used to melt and accelerate powder particles. A special feature of this plant is its ability to accelerate powder particles to supersonic speeds, reaching values of up to 700 m/s. It is important to note that the flame temperature in this setup is much lower than in the case of using a plasma jet (about 3000 K instead of about 15,000 K) [45,46]. Figure 1b shows a schematic diagram of the installation of the HVOF Termika-3 system. Propane (C_3H_8) and oxygen (O) in cylinders, which are combustible gases, were used as fuel. With the gas control panel, the pressure of these gases is set. At high pressure, these gases are mixed with each other in a chamber, and then the powders are fed into the burner using a conveying gas (compressed air from a compressor) from a powder dispenser. At the outlet of the burner, the powders enter the flame where they are melted to a plastic state. Then, the melted powders are directed to the pre-prepared surface (substrate), forming a coating.

**Figure 1.** The process of spraying samples using the HVOF Termika-3 method (a) and a schematic representation of the HVOF Termika-3 method (b).

Metal–ceramic coatings 86WC-10Co-4Cr were obtained on HVOF Termika-3 with varying spraying distance: L1-100 mm, L2-200 mm, and L3-300 mm. The dwell time of all samples during spraying was 15 s. The parameters established for HVOF Termika-3 high-velocity oxygen–fuel spraying were determined by conducting a series of experiments and are summarized in Table 2.

Structural studies and measurements of porosity and microhardness of the coatings were carried out on cross-sectional microslides. The morphology of the powder and cross-section of the coatings was characterized by TESCAN MIRA3 LMH scanning electron microscopy (TESCAN, Brno, Czech Republic) with the INCA ENERGY energy dispersion

analysis set-top box (“Oxford Instruments”, Abingdon, UK). The porosity of coatings was evaluated by SEM images using image analysis software Altami Studio 4.0 of optical microscope Altami MET 5S (Altami LLC, St. Petersburg, Russia). The SEM observations of the initial powders show that the powders have a spherical shape (Figure 2a). This is important from a technological point of view, as it provides a suitable bulkiness for the powder particles during spraying. According to the SEM image analysis of the powder cross-section (Figure 2b), it was found that, morphologically, the structure consists of two phases with different colors, where the polygonal WC particles have a light color and the metallic cobalt–chromium phase (matrix) is represented in a dark gray color. The tungsten carbide particles are well distributed and embedded in the cobalt–chromium matrix, which is in agreement with many studies in the reported literature [47,48]. It can also be observed that pores are present, which may facilitate heat distribution and promote the better melting or semi-melting of the particles. The X-ray diffraction analysis (XRD) of powders and coatings was performed on a Cu-K α -emitting X’PertPRO diffractometer (Philips Corporation, Amsterdam, The Netherlands) ($\lambda = 0.154$ nm) operated at a voltage and current of 40 kV and 30 mA, respectively. Measurements were performed over a 2θ range from 10° to 100° , and for the experiments, the width and exposure time were set to 0.05° and 3 s for each step. The diffractograms were interpreted using the full-profile analysis program POWDER CELL (version 2.4). The surface roughness of the coatings was determined using a profilometer model 130 (JSC “Plant PROTON”, Moscow, Russia) on an average of five measurements. The measurement of microhardness of samples was carried out on the cross-section of the coatings (10 measurements for each type of coating) on a microtweedometer Metolab 502 (Metolab, Russia), under indenter loads of $m = 100$ g and a dwell time of 10 s. Tribological tests on friction and wear were carried out on a Tribometer TRB³ (Anton-Paar, Buchs, Switzerland) using the standard “ball-on-disk” method, where a steel ball with a diameter of 6.0 mm coated with 100Cr6, with a load of 10 N, a linear velocity of 3 cm/s, a radius of curvature of wear 2 mm, and a friction path of 100 m is used as a counterbody.

Table 2. Spraying regimes for 86WC-10Co-4Cr coatings.

Sample code	L1	L2	L3
Spray distance, mm	100	200	300
Parameter regimes on the gas control panel		Optimal values	
Propane pressure		2.9 Bar	
Oxygen pressure		5.0 Bar	
Compressed air pressure		3.2 Bar	

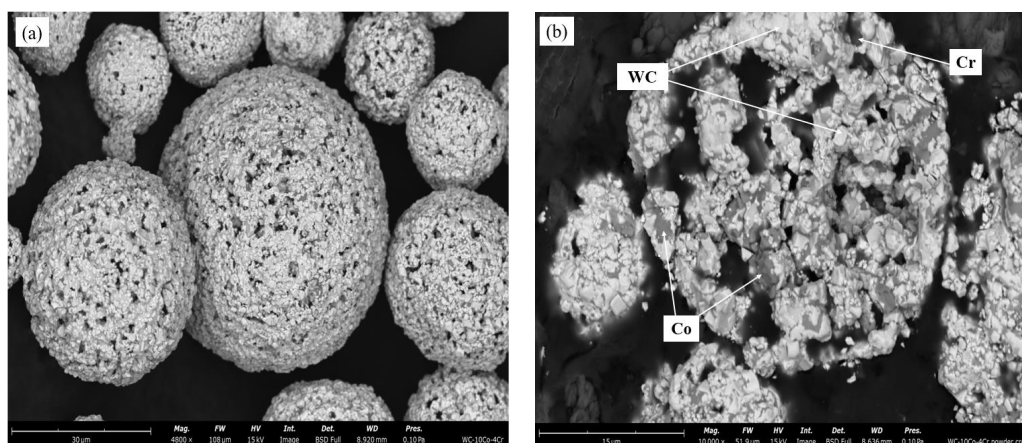


Figure 2. Agglomerated and sintered WC-10Co-4Cr powder: (a) morphology of initial powder; (b) cross-section of powder agglomerate.

3. Results and Discussion

Figure 3 shows the results of the study of the phase composition of powder and 86WC-10Co-4Cr metal–ceramic coatings obtained by the HVOF method at different spraying distances (L1-100 mm, L2-200 mm, L3-300 mm). X-ray diffraction analysis shows that the initial WC-10Co-4Cr powder consists of the main phase of higher tungsten carbide (WC), as well as tungsten (W), cobalt (Co) and η phases— $\text{Co}_3\text{W}_3\text{C}$ ($\text{Co}_6\text{W}_6\text{C}$). The distributions of the η phase are reflected in the X-ray diffraction spectrum only in the low angle region. When the powder was exposed to HVOF flame, some changes in the X-ray diffraction pattern were observed. The WC phase, the lower tungsten carbide (W_2C) phase, and the cobalt oxide (CoO) phase, of which the latter two were found in the coatings, were obtained from the thermal decomposition of the powder during spraying, which is in agreement with a previous study [49]. Based on the diagram of state of the double system W-C, it can be assumed that in the temperature range of 2400–2800 °C, there is a loss of carbon from the WC phase, which leads to the formation of the brittle W_2C phase [50]. And the formation of oxide phase CoO is explained by the fact that during high-speed gas–flame spraying, an oxygen–propane mixture was used for the oxidizing gas–flame environment, which leads to the more intensive interaction of WC with oxygen. This results in a partial loss of carbon; thus, the excess carbon formed by the dissolution of WC diffuses into the metal matrix and forms another carbide (W_2C) and oxide (CoO) phase.

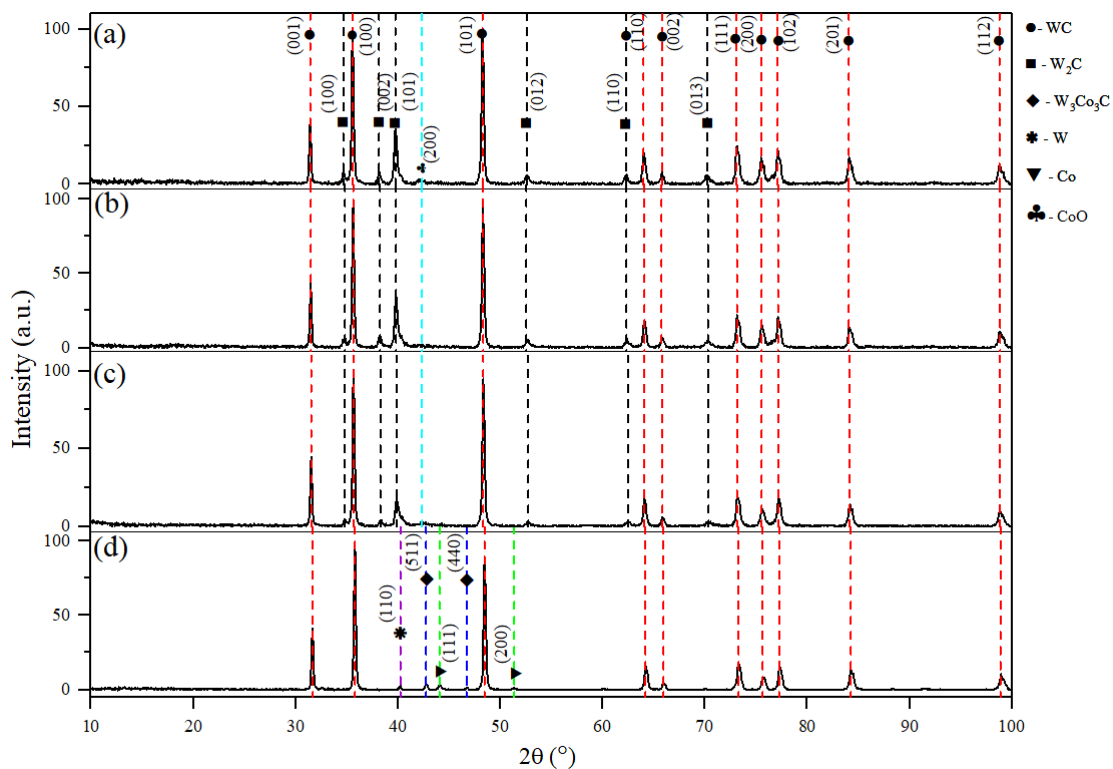


Figure 3. Diagrams of WC-10Co-4Cr powders and coatings at different spraying distances. (d) 86WC-10Co-4Cr powder; 86WC-10Co-4Cr coatings ((a) L1; (b) L2; (c) L3).

At 300 mm, it can be seen that the intensity of the lower W_2C decreases, indicating that the HVOF process at low temperature and high speed can effectively prevent decarburization. Also, it can be observed that in the diffractogram of Figure 3c, there are no η reflections of $\text{Co}_3\text{W}_3\text{C}$ phase because it was unstable during HVOF spraying, which is also confirmed by another study [51].

Table 3 shows the data on the phase composition of the coatings analyzed by the POWDERCELL full profile analysis program (version 2.4). The experimental and calculated diffractograms were compared graphically, and the phase content in each coating, phase

lattice parameters, coherent scattering regions (CSR) of the crystal, and microstress values ($\Delta d/d \times 10^{-3}$) were determined. According to the phase composition analysis (Table 3) and XRD (Figure 3), the following phases were found in the coatings: WC, W_2C , and CoO. In all coatings, the crystallite size calculated using POWDERCELL program for WC phase is about 44 nm, while for W_2C and CoO phases it was different, as shown in Table 3. Based on the full X-ray profile analysis of the 86WC-10Co-4Cr coatings, the content percentages of individual phases were also determined. The content percentages of the WC phases in all L1, L2, and L3 coatings were 51%, 55%, 57%, and for the W_2C phase, they were 21%, 19%, and 11%, respectively. It can be observed that the content of CoO phase in the coating at 100 mm distance was higher than the other coatings. This indicates that at close spacing, the coating is more susceptible to oxidation under the influence of high temperatures. The low W_2C content in the L3 coating indicates a low degree of decomposition of WC to W_2C , it can be assumed that as the spraying distance increases, the powder is less at high temperature since, the flame temperature decreases with increasing distance.

Table 3. Results of X-ray phase analysis.

Sample	Detected Phases	Phase Content, Wt. %	Lattice Parameters,	Size of CSA, nm	$\Delta d/d \times 10^{-3}$
Coating L1	WC	51	a = 2.9012 c = 2.8321	41	0.552
	W_2C	21	a = 2.9717 c = 4.6936	28	2.234
	CoO	38	a = 4.2516	21	5.057
Coating L2	WC	55	a = 2.9015 c = 2.8317	39	0.723
	W_2C	19	a = 2.9721 c = 4.6936	33	3.517
	CoO	26	a = 4.2666	22	1.664
Coating L3	WC	57	a = 2.9015 c = 2.8320	44	0.037
	W_2C	11	a = 2.9687 c = 4.6876	31	1.7
	CoO	22	a = 4.2654	8	1.581

Crystallographic parameters and phase identifications were taken from the ICDD PDF-2 database using the POWDERCELL full-profile analysis program (version 2.4). For the CoO and Co_3W_3C phases, data from the Inorganic Crystal Structure Database (ICSD) were used. The detailed results are summarized in Table 4.

Table 4. Crystallographic parameters of phases.

Phase	Crystal Lattice	Cardboard	Spatial Group
WC	Hexagonal	00-025-1047	P-6m2
W_2C	Hexagonal	00-035-0776	P-3m1
W	Cubic	00-004-0806	Im3m
Co	Cubic	00-015-0806	Fm3m
CoO	Cubic	ICSD 245320	Fm3m
Co_3W_3C	Cubic	ICSD 617462	Fd3m

Figure 4 shows the cross-sectional morphology of the coatings obtained with varying spraying distances: L1—100 mm; L2—200 mm; L3—300 mm. All coatings are tightly adhered to the substrate without any cracks and failures and no signs of delamination were

observed. For convenience, the analysis was carried out at different magnifications to obtain more detailed information about the coating structure and evaluation of its characteristics.

The thickness of the three coatings varied from 1.35 mm to 630 μm . It was found that the thickness of the metal–ceramic coating decreases with increasing spraying distance: $h = 1.35\text{ mm}$; $h = 1.15\text{ mm}$; and $h = 630\text{ }\mu\text{m}$ for samples L1, L2, and L3, respectively. The porosity of coatings was estimated by SEM images using Altami Studio 4.0 software for image analysis. In all coatings, the relative porosity did not exceed 2.5%; however, the lowest porosity with a value of 0.7% was shown by the coating obtained at a spraying distance of 300 mm (Figure 4c). The formation of porous and low porous structures in coatings may depend on various factors. First, it can be related to the more efficient heating of the powder to the plastic state during the spraying process. That is, the more intense heating of the powder at longer spraying distance may favor the formation of a more compact coating with reduced porous properties. Second, as the spraying distance from the atomizer to the substrate increases, the flame area expands. Thus, the powder particles are spread over a larger area of the substrate and are more likely to cover the entire substrate surface uniformly, which is characterized by a dense and homogeneous microstructure. This dense structure is due to the characteristic feature of the HVOF process (mainly the high kinetic energy of the particles) [48,52]. As the SEM analysis shows, at a spraying distance of 100 mm, significant and distinct micropores were formed in the microstructure of the coating. This is probably due to two factors: firstly, the overheating of powder particles due to excessively high flame temperature; secondly, the short-term stay of particles in the flame, which does not allow the uniform distribution and melting of the particles. The above factors lead to a non-uniform coating and the formation of micropores. From the SEM analysis of the cross-sections of all coatings (Figure 4d–f), it can be observed that the tungsten carbide (WC) particles are uniformly distributed in the matrix phase (CoCr). The dark gray color is probably the cobalt–chromium CoCr matrix, and the light gray particles represent tungsten carbide (WC). The Co binder, however, showed a uniform distribution in the main WC phase. There is a possibility that the lower tungsten carbide (W_2C) may be dispersed in this cobalt binder, as shown in Figure 4d. This assumption is supported by X-ray diffraction analyses, as shown in Figure 3a–c, where the dispersed phase contains tungsten and is deficient in cobalt. Most of the WC parts retained their polygonal, white-colored shape. According to numerous studies, the formation of W_2C around WC is attributed to the decarburization of WC during the HVOF process [53–55].

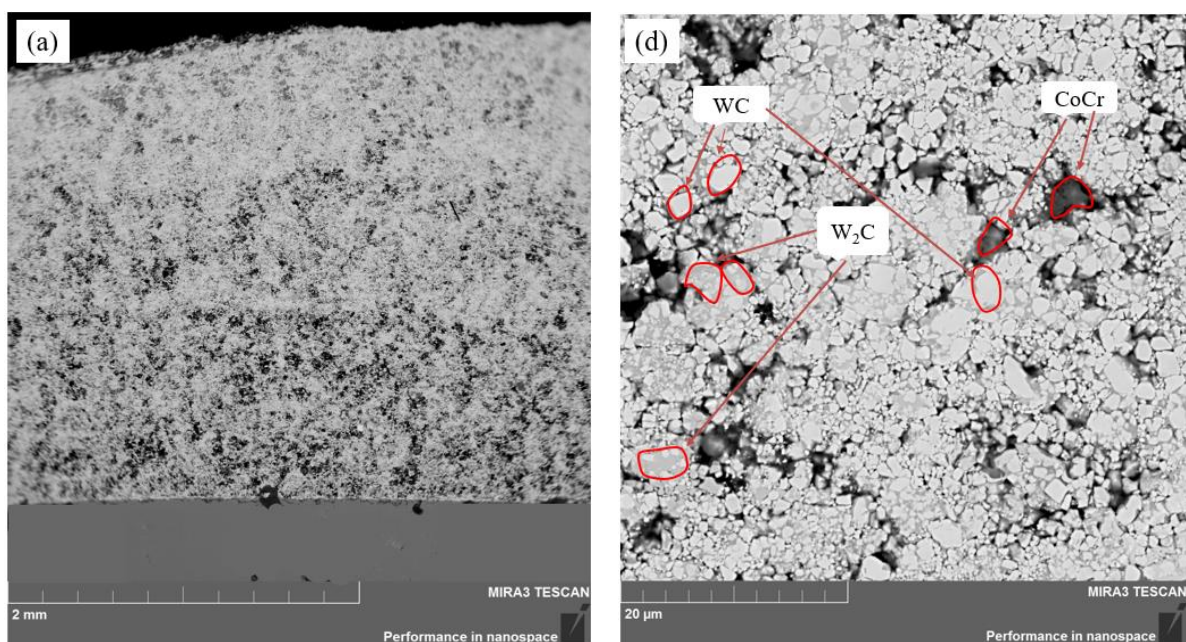


Figure 4. Cont.

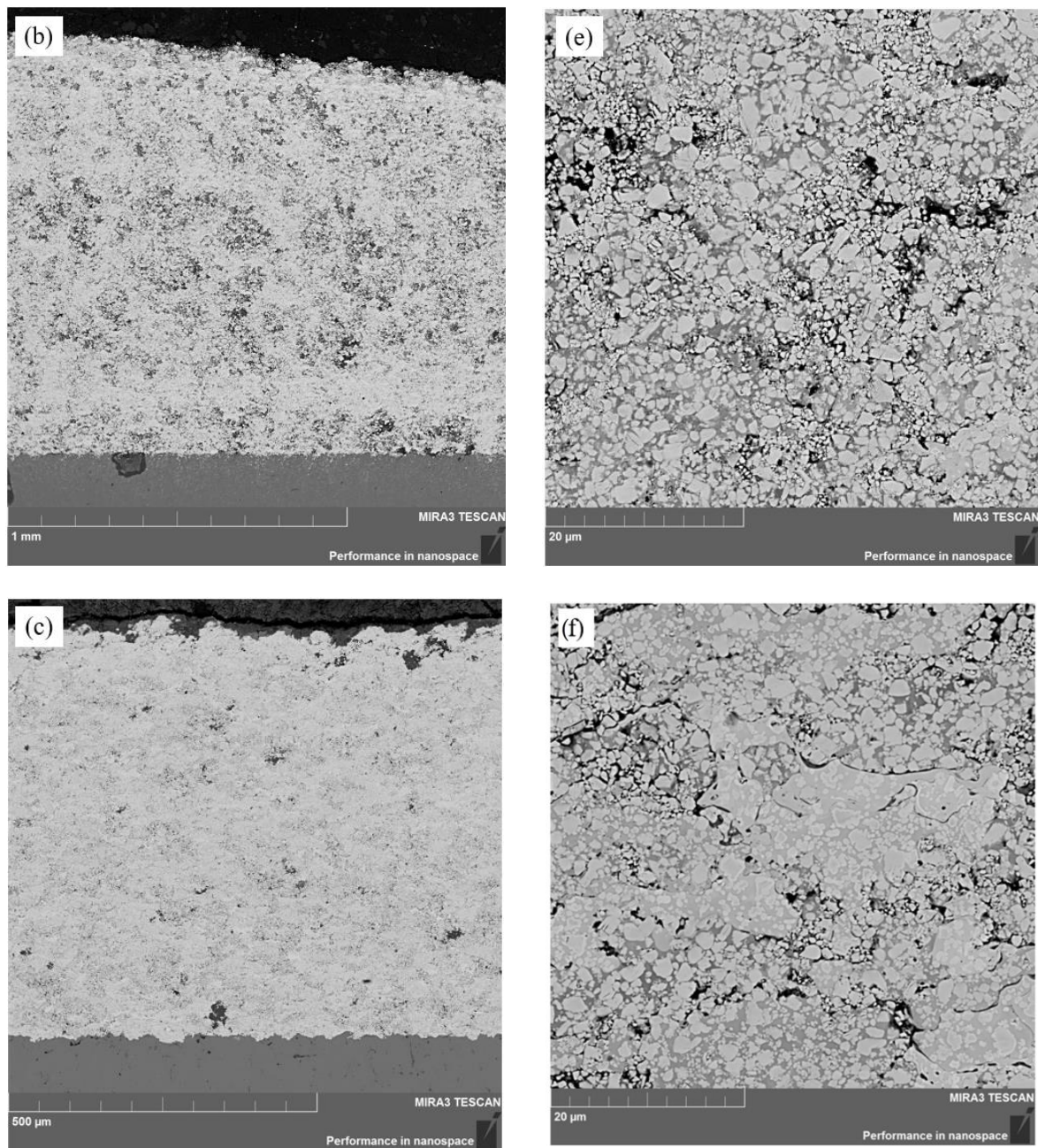


Figure 4. SEM images of the cross-sectional morphology of 86WC-10Co-4Cr coatings obtained by varying the spraying distance. (a,d) 100 mm; (b,e) 200 mm; (c,f) 300 mm.

Figure 5 shows the results of the elemental mapping analysis of the cross-section of the coatings obtained through varying spraying distances: L1—100 mm; L2—200 mm; and L3—300 mm. The EDS analysis of the cross-sections demonstrated the presence of several elements such as W, C, O, Co, and Cr, while the 30×13 corrosion-resistant steel substrate contains the elements Fe and C. The mapping analyses in Figure 5a–c illustrate that the inner layers of the coatings are more susceptible to oxidation than the coating obtained at 300 mm spraying distance. This is due to the fact that high-speed gas-flame spraying utilizes an oxygen–propane mixture for the gas-flame oxidizing environment, which leads to a more intense interaction of WC with oxygen. This results in a partial loss of carbon; thus, the excess carbon resulting from the dissolution of WC diffuses into the metal matrix and forms another carbide phase (W_2C). From the coatings L1 and L2 (Figure 5a–c), we can see the oxidation process caused by the high temperature of the

particles during the spraying process. At higher temperatures, the particles have more energy, which accelerates the chemical reactions, including oxidation. This results in a more intense formation of oxide shells around the WC particles. This is especially noticeable when spraying in an oxidizing environment where oxygen stimulates oxidation processes. Higher flame temperatures and the longer stay of particles in the flame can cause more complete oxidation. But in our case, partial oxidation occurred on the coatings L1 and L2 because oxides occupy the places where the pores are located (Figure 5a,b). Moreover, as mapping analyses show, in coating L3, there are more oxides on the surface than in the other two coatings (L1 and L2), which may be due to the lower flame temperature (flame temperature decreases with increased spraying distance).

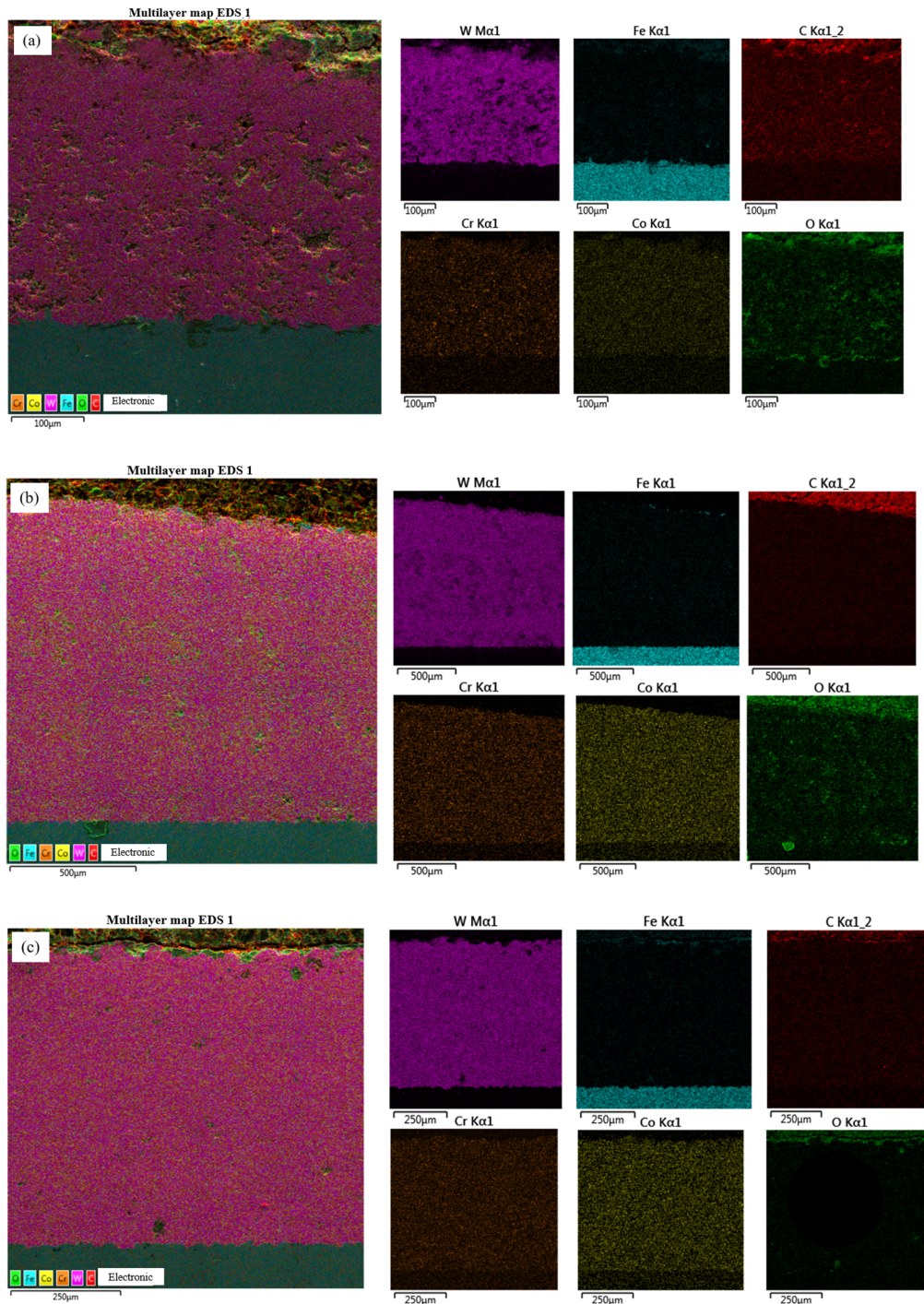
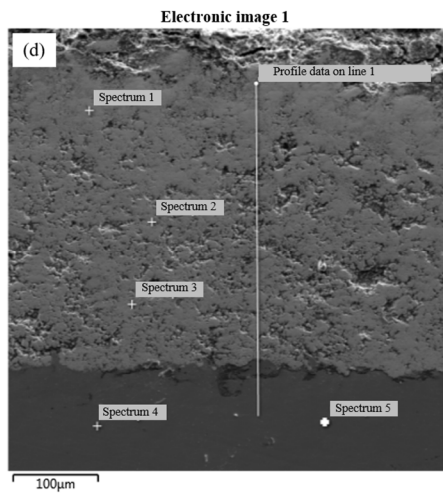
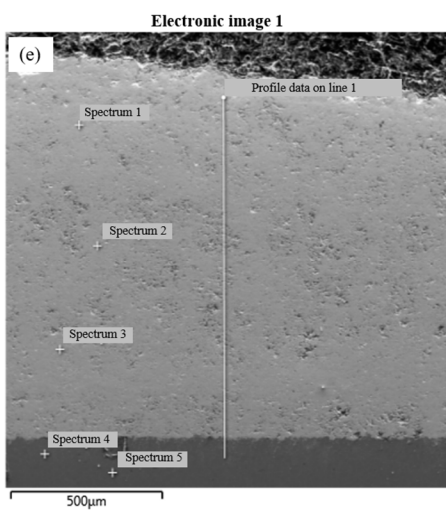


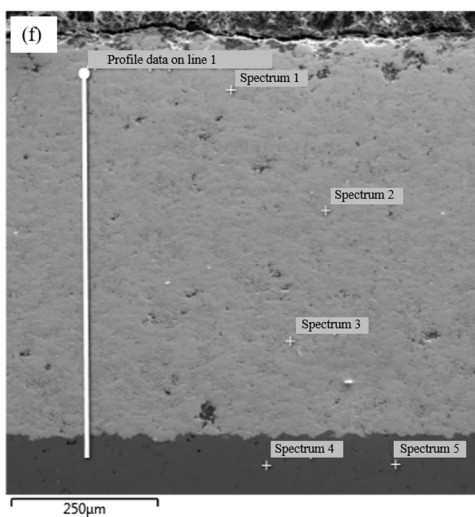
Figure 5. Cont.



Coatings (wt%)	W	C	Fe	O	Co	Cr
Spectrum 1	68.3	18.1		0.9	10.1	2.6
Spectrum 2	55.9	12.4		5.9	19.3	4.9
Spectrum 3	79.1	18.6		1.5	0.8	
Spectrum 4	2.2	14.3	81.4	1.0		1.0
Spectrum 5		15.0	83.2	0.9		0.9



Coatings (wt%)	W	C	Fe	O	Co	Cr
Spectrum 1	71.5	16.9		1.3	6.5	3.9
Spectrum 2	42.0	13.2		2.2	22.0	8.7
Spectrum 3	56.7	14.3		3.6	18.2	7.2
Spectrum 4	5.5	13.5	77.4	2.5		1.0
Spectrum 5	2.1	13.3	83.0	0.6		1.0



Coatings (wt%)	W	C	Fe	O	Co	Cr
Spectrum 1	81.7	16.8		0.4	0.7	
Spectrum 2	79.3	17.2		0.5	2.8	
Spectrum 3	61.3	17.1		0.2	16.7	4.2
Spectrum 4		13.0	85.3	0.1		1.1
Spectrum 5		13.0	85.2	0.2		1.2

Figure 5. Elemental distribution maps of sprayed elements in the analyzed area of the 86WC-10Co-4Cr coating. (a) L1—100 mm; (b) L2—200 mm; (c) L3—300 mm; and elemental spot analysis; (d) L1—100 mm; (e) L2—200 mm; (f) L3—300 mm.

Elemental point analysis was performed in all coatings in three different areas (Figure 5d–f). The elements W, C, and Co, which were distributed throughout the coating, were observed at each point where the analysis was carried out. It was observed that oxide (O) was almost absent in the L3 coating structure as it does not exceed the threshold of 0.4 (Figure 5f). The low oxide content in the L3 coating structure was mentioned above. Speaking from a general point of view, the point map analysis revealed areas with increased concentration of individual chemical elements in the analyzed coatings (L1, L2, L3): the highest concentration was tungsten and also carbon.

In Figure 6, it is possible to study the distribution of elements along the coating cross-sectional line. Along the line drawn across all three coatings (L1, L2, L3), a uniform distribution of tungsten can be seen. It can be seen that coating L1 showed the most oxide distribution from the center to the substrate along the line (as depicted in Figure 6a). Chemical analysis also confirmed that coating L1 had the highest oxide content within the coating compared to the other coatings L2 and L3 (Figure 6a,b). In the other coatings (Figure 6b,c), it can be seen that as the spraying distance increases, the oxygen starts to decrease in the coatings along the line. Thus, no oxides were detected along the line drawn in the structure of coating L3.

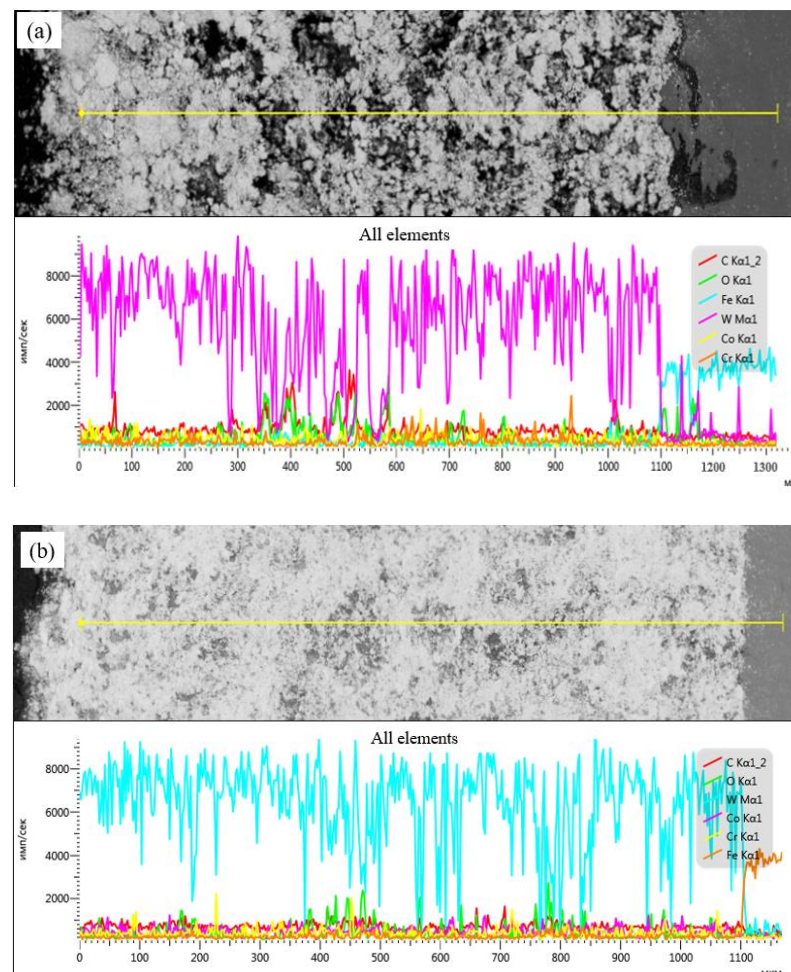


Figure 6. Cont.

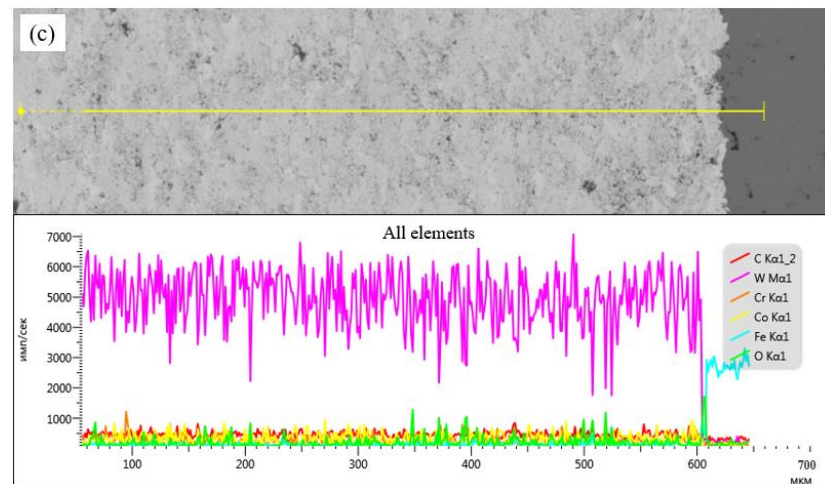


Figure 6. Distribution of elements along the cross-sectional line of the 86WC-10Co-4Cr metal–ceramic coating. (a) L1—100 mm; (b) L2—200 mm; (c) L3—300 mm.

Figure 7 shows the results of surface roughness measurements of coatings obtained by high-speed gas–flame spraying at different spraying distances (L1, L2, L3). Studies on coating roughness have showed that changing the spraying distance from 100 mm to 300 mm affects the roughness parameter; the average values of which were 1.73, 1.93, and 2.03 μm , respectively. As the spraying distance increased, the roughness of the coatings increased. In addition, as the sputtering distance increased and the temperature of the flying particles in the flame decreased, resulting in an increase in the number of cold particles outside the hot center of the flame. This results in a developed coating surface characterized by high roughness.

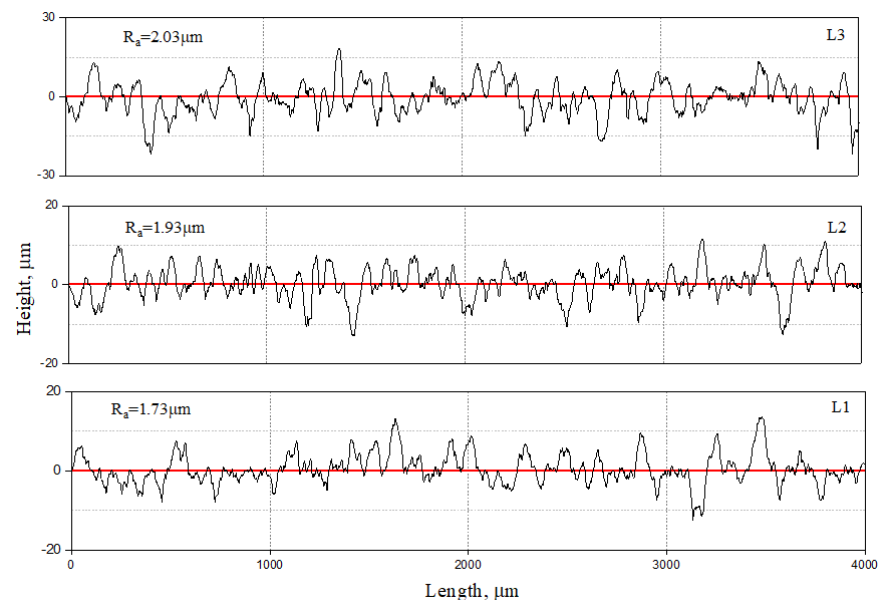


Figure 7. Surface roughness of the 86WC-10Co-4Cr coating. L1—100 mm; L—200 mm; L3—300 mm.

The results of the measurements of average values of the microhardness of coatings depending on the spraying regime showed that increasing the distance of spraying leads to an increase in the values of the microhardness of coatings: L1— 755 ± 16 ; L2— 797 ± 11 ; and L3— 976 ± 17 . This can be explained by several factors, one of which is the increase in the volume fraction of carbides in the coating when the spraying distance is increased up to 300 mm. The results are in agreement with a previous study [56], i.e., the higher the degree of decarburization, the lower the hardness. And, so, the successive decrease in spraying

distance from 300 to 100 mm is accompanied by a slight decrease in microhardness from 976 ± 17 to 755 ± 16 HV_{0.1}. This indicates that at a spraying distance of 100 mm, the coating becomes softer. The results of the study also agree with the XRD analysis data (Table 3), which indicates the presence of high concentrations of W₂C phase in the coatings obtained at spraying distances of 100 and 200 mm.

The graph showing the dependence of the friction coefficient on the friction path and dependence of wear volume on the sputtering distance is presented in Figure 8a,b. It is established that with the increase in spraying distance, the friction coefficient and the wear volume of metal–ceramic coating 86WC-10Co-4Cr decreases: $\mu = 0.488$; $\mu = 0.485$; and $\mu = 0.463$ and $v = 0.079$ mm³; $v = 0.043$ mm³; and $v = 0.036$ mm³ for samples L1, L2, and L3, respectively (Figure 8a,b). Figure 8b shows that the maximum wear resistance is characteristic of the coating obtained at a spraying distance of 300 mm; the minimum for the sample obtained at a spraying distance of 100 mm. The decrease in wear resistance can be explained by a decrease in the content of the WC phase.

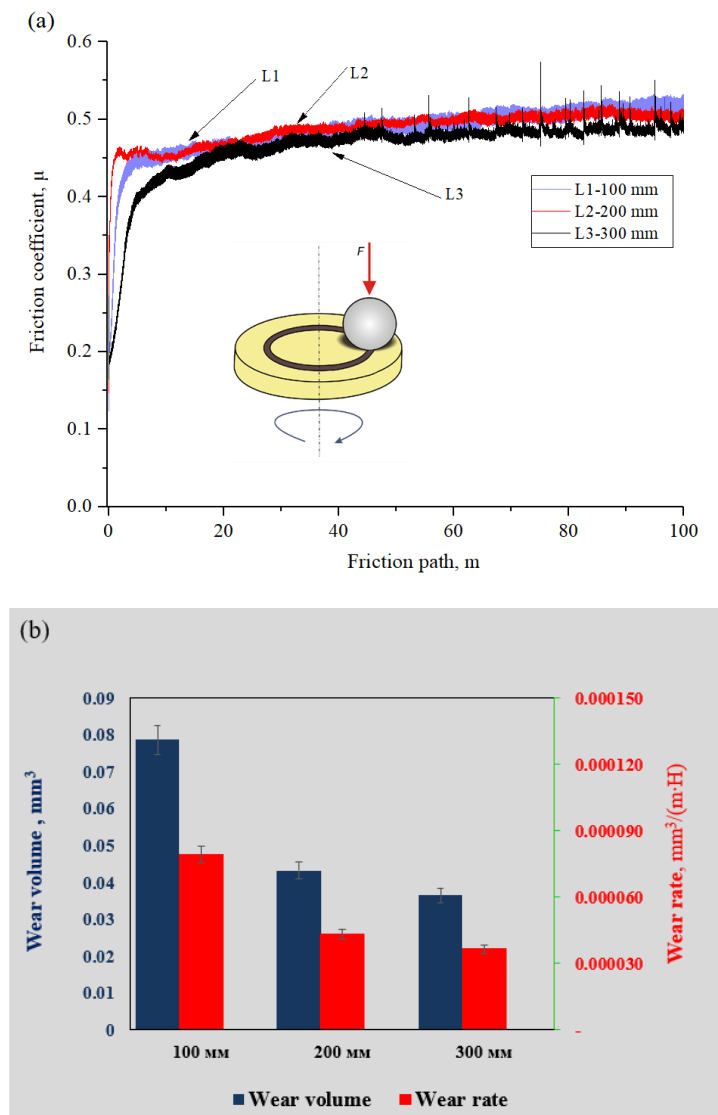


Figure 8. Graph of dependence of friction coefficient on friction path (a) and dependence of wear volume on spraying distance (b).

4. Conclusions

The following conclusions can be reached in this study:

Increasing the spraying distance allowed the formation of high quality 86WC-10Co-4Cr metal–ceramic coatings characterized by high density and an absence of cracks and oxide areas in the structure of L3 coatings.

The porosity of the coatings did not exceed 2.5%. The lowest porosity with a value of 0.7% was shown by the coating obtained at a spraying distance of 300 mm.

The thickness of all the coatings ranged from 1.35 mm to 630 μm . It was found that the average thickness of the metal–ceramic coating decreased with increasing spraying distance.

According to the data obtained by SEM and elemental mapping, all coatings consist of WC and W₂C particles uniformly distributed in the Co-Cr metal matrix. On the elemental map of coatings obtained at distances of 100 and 200 mm, partial regions saturated with oxygen can be identified, which are associated with an oxidizing environment where oxygen stimulates oxidation processes. And at a distance of 300 mm, the total oxide content in the coating structure did not exceed 0.4%, which may be due to the lower flame temperature (flame temperature decreases with increasing sputtering distance).

X-ray diffraction analysis showed that the spraying distance has a significant effect on the proportion of the CoO and lower W₂C phases. As the spraying distance increased, the content of oxide and low carbide phases decreased. The phase composition of the metal–ceramic coatings consisted of hexagonal WC, hexagonal W₂C, and cubic cobalt oxide (CoO).

It was found that the maximum microhardness (976HV0.1) is characteristic of the L3 coating, and the minimum values of microhardness are observed in the L1 and L2 coatings, which can be explained by the increase in the WC phase fraction with the increasing spraying distance.

With the increase in spraying distance, there were increases in the roughness of the coatings, namely 1.73 μm , 1.93 μm , and 2.03 μm for samples L1—100 mm, L2—200 mm and L3—300 mm, respectively.

It was revealed that the maximum wear resistance is characteristic of the coating obtained at a sputtering distance of 300 mm (wear volume, 0.036 mm³), and the minimum wear resistance is characteristic of the coating obtained at a distance of 100 mm ($v = 0.079 \text{ mm}^3$).

Author Contributions: B.R. and N.M.: formal analysis, supervision, writing—review and editing; D.K. and M.A.: investigation, methodology; S.K. and S.A.: resources, data curation. All authors have read and agreed to the published version of the manuscript.

Funding: This study was funded by the Committee of Science of the Ministry of Science and Higher Education of the Republic of Kazakhstan (grant no. AP14870977).

Institutional Review Board Statement: Not applicable.

Informed Consent Statement: Not applicable.

Data Availability Statement: Data are contained within the article.

Conflicts of Interest: Author Nazerke Muktanova and Daur Kakimzhanov were employed by the company PlasmaScience LLP. The remaining authors declare that the research was conducted in the absence of any commercial or financial relationships that could be construed as a potential conflict of interest.

References

1. Sherov, K.T.; Gabdysalyk, R. Analysis and study of the problem of manufacturing large gate valves for main pipelines. In Proceedings of the University; Publishing House of Karaganda State Technical University: Karaganda, Kazakhstan, 2018; Volume 70, pp. 13–17. (In Russian).
2. Available online: <https://www.youtube.com/watch?v=wg5IZN2noH0> (accessed on 21 August 2017).
3. Available online: <https://www.uzpa.kz/about/> (accessed on 15 September 2015).

4. Poloskov, S.C. Problems of cladding of sealing surfaces of pipeline valves and ways of their solution. *Bull. Don State Techn. Univ.* **2019**, *19*, 349–356. (In Russian)
5. Tukov, S.A.; Korchagina, M.V.; Kireev, S.O. *Problems of Tightness of Ball Valves and Methods of Their Solution*; Don State Technical University: Rostov-on-Don, Russia, 2018; pp. 12–15.
6. Available online: <http://www.indmet.ru/tech/vyisokoskorostnoe-gazotermicheskoe-napyilenie-hvof> (accessed on 17 June 2017).
7. Keshavamurthy, R.; Sudhan, M.D.; Kumar, A.; Ranjan, V.; Singh, P.; Singh, A. Wear behaviour of hard chrome and tungsten carbide-HVOF coatings. *Mater. Proc.* **2018**, *5*, 24587–24594. [[CrossRef](#)]
8. Kumar, H.; Chittosiya, C.; Shukla, V.N. HVOF Sprayed WC Based Cermet Coating for Mitigation of Cavitation, Erosion & Abrasion in Hydro Turbine Blade. *Mater. Today Proc.* **2018**, *5*, 6413–6420. [[CrossRef](#)]
9. Li, G.P.; Peng, Y.B.; Yan, L.W.; Xu, T.; Long, J.Z.; Luo, F.H. Effects of Cr concentration on the microstructure and properties of WC-Ni cemented carbides. *J. Mater. Res. Technol.* **2020**, *9*, 902–907. [[CrossRef](#)]
10. Druzhnova, Y.S. Development of methods of gas-thermal spraying of hardening coatings based on tungsten and chromium carbides (review). *Proc. VIAM* **2022**, *116*, 100–115. (In Russian)
11. Yu, J.; Liu, X.; Yu, Y.; Li, H.; Liu, P.; Huang, K.; Sun, R. Research and Application of High-Velocity Oxygen Fuel Coatings. *Coatings* **2022**, *12*, 828. [[CrossRef](#)]
12. Samodurova, M.; Shaburova, N.; Samoilova, O.; Moghaddam, A.O.; Pashkeev, K.; Ul'yanitskiy, V.; Trofimov, E. Properties of WC–10%Co–4%Cr Detonation Spray Coating Deposited on the Al–4%Cu–1%Mg Alloy. *Materials* **2021**, *14*, 1206. [[CrossRef](#)]
13. Ghadami, F.; Sabour Rouh Aghdam, A. Improvement of high velocity oxy-fuel spray coatings by thermal post-treatments: A critical review. *Thin Solid Films* **2019**, *678*, 42–52. [[CrossRef](#)]
14. Hong, S.; Wu, Y.P.; Wang, Q.; Ying, G.B.; Li, G.Y.; Gao, W.W.; Wang, B.; Guo, W.M. Microstructure and Cavitation-Silt Erosion Behavior of High-Velocity Oxygen-Fuel (HVOF) Sprayed Cr₃C₂-NiCr Coating. *Surf. Coat. Technol.* **2013**, *225*, 85–91. [[CrossRef](#)]
15. Gui, M.; Eybel, R.; Asselin, B.; Radhakrishnan, S.; Cerps, J. Influence of Processing Parameters on Residual Stress of High Velocity Oxy-Fuel Thermally Sprayed WC-Co-Cr Coating. *J. Mater. Eng. Perform.* **2012**, *21*, 2090–2098. [[CrossRef](#)]
16. Murthy, J.K.N.; Venkataraman, B. Abrasive wear behaviour of WC–CoCr and Cr₃C₂-20(NiCr) deposited by HVOF and detonation spray processes. *Surf. Coat. Technol.* **2006**, *200*, 2642–2652. [[CrossRef](#)]
17. Wheeler, D.W.; Wood, R.J.K. Erosion of hard surface coatings for use in offshore gate valves. *Wear* **2005**, *258*, 526–536. [[CrossRef](#)]
18. Ulmanu, V.; Bădicioiu, M.; Călțaru, M.; Zecheru, G.; Draghici, G.; Minescu, M.; Preda, C. Research regarding the hard-facing of petroleum gate valves by using high velocity oxygen fuel technology. *J. Balkan Tribol. Assoc.* **2010**, *16*, 551–557.
19. Caltaru, M.; Bădicioiu, M.; Ripeanu, R.G. Establishing the tribological behaviour of HVOF hardfacing applied at petroleum gate valves. *J. Balkan Tribol. Assoc.* **2013**, *19*, 448–460.
20. Tan, S.; Wharton, J.A.; Wood, R.J.K. Solid Particle Erosion Corrosion Behaviour of a Novel HVOF Nickel Aluminium Bronze Coating for Marine Applications-Correlation Between Mass Loss and Electrochemical Measurements. *Wear* **2005**, *258*, 629–640. [[CrossRef](#)]
21. Thakur, L.; Arora, N. Sliding and Abrasive Wear Behavior of WC-CoCr Coatings With Different Carbide Sizes. *J. Mater. Eng. Perform.* **2013**, *22*, 574–583. [[CrossRef](#)]
22. Zo, W.; Skrzypek, S.J. Tribological Properties of Plasma and HVOF-Sprayed NiCrBSi-Fe₂O₃ Composite Coatings. *Surf. Coat. Technol.* **2013**, *220*, 282–289. [[CrossRef](#)]
23. Yu, Y.; Wu, Y.; Hong, S.; Cheng, J.; Zhu, S.; Li, H. Microstructure and wear behavior of the (AlCoCrFeNi)_x/(WC–10Co)_{1-x} composite coatings produced via high velocity oxy-fuel thermal spraying. *Ceram. Int.* **2023**, *49*, 28560–28570. [[CrossRef](#)]
24. Ding, X.; Cheng, X.-D.; Shi, J.; Li, C.; Yuan, C.-Q.; Ding, Z.-X. Influence of WC size and HVOF process on erosion wear performance of WC-10Co4Cr coatings. *Int. J. Adv. Manuf. Technol.* **2018**, *96*, 1615–1624. [[CrossRef](#)]
25. Song, B.; Pala, Z.; Voisey, K.; Hussain, T. Gas and liquid-fuelled HVOF spraying of Ni50Cr coating: Microstructure and high temperature oxidation. *Surf. Coat. Technol.* **2017**, *318*, 224–232. [[CrossRef](#)]
26. Holcomb, G.R. Calculation of reactive-evaporation rates of chromia. *Oxid. Metals* **2008**, *69*, 163–180. [[CrossRef](#)]
27. Karimi, A.; Verdon, C.; Barbezat, G. Microstructure and hydroabrasive wear behaviour of high-velocity oxy-fuel thermally sprayed WC–Co (Cr) coatings. *Surf. Coat. Technol.* **1993**, *57*, 81–87. [[CrossRef](#)]
28. Kim, H.J.; Kweon, Y.G.; Chang, R.W. Wear and Erosion Behavior of Plasma-Sprayed WC-Co Coatings. *J. Thermal Spray Technol.* **1994**, *3*, 169–178. [[CrossRef](#)]
29. Suresh Babu, P.; Basu, B.; Sundararajan, G. Abrasive Wear Behavior of Detonation Sprayed WC-12Co Coatings: Influence of Decarburization and Abrasive Characteristics. *Wear* **2010**, *268*, 1387–1399. [[CrossRef](#)]
30. Kumari, K.; Anand, K.; Bellacci, M.; Giannozzi, M. Effect of Microstructure on Abrasive Wear Behavior of Thermally Sprayed WC-10Co-4Cr Coatings. *Wear* **2010**, *268*, 1309–1319. [[CrossRef](#)]
31. Maharajan, S.; Michael Thomas Rex, F.; Ravindran, D.; Rajakarunakaran, S. Erosive and corrosive wear performance and characterization studies of plasma-sprayed WC/Cr₃C₂ coating on SS316. *Appl. Ceramic Technol.* **2022**, *19*, 2845–2861. [[CrossRef](#)]
32. Bhosale, D.G.; Ram Prabhu, T.; Rathod, W.S. Sliding and erosion wear behaviour of thermal sprayed WC-Cr₃C₂-Ni coatings. *Surf. Coat. Technol.* **2020**, *400*, 126192. [[CrossRef](#)]
33. Vats, A.; Patnaik, A.; Meena, M.L.; Shringi, D. Role of microfactors on microstructure and on the tribological performance of HVOF coatings: A review. *IOP Conf. Ser. Mater. Sci. Eng.* **2021**, *1017*, 012010–012016. [[CrossRef](#)]

34. Robert, J.K.; Wood, S.; Herd, M.R. A critical review of the tribocorrosion of cemented and thermal sprayed tungsten carbide. *Tribol. Int.* **2018**, *119*, 491–509. [[CrossRef](#)]
35. Zhou, W.X.; Zhou, K.S.; Li, Y.X.; Deng, C.M.; Zeng, K.L. High temperature wear performance of HVOF-sprayed Cr₃C₂-WC-NiCoCrMo and Cr₃C₂-NiCr hardmetal coatings. *Appl. Surf. Sci.* **2017**, *416*, 33–44. [[CrossRef](#)]
36. Gopi, R.; Saravanan, I.; Devaraju, A.; Ponnusamy, P. Tribological behaviour of thermal sprayed high velocity oxy-fuel coatings on tungsten carbide—A review. *Mater. Today Proc.* **2020**, *39*, 292–295. [[CrossRef](#)]
37. Picas, J.A.; Xiong, Y.; Punset, M.; Ajdelsztajn, L.; Forn, A.; Schoenung, J.M. Microstructure and wear resistance of WC–Co by three consolidation processing techniques. *Int. J. Refract. Metals Hard Mater.* **2009**, *27*, 344–349. [[CrossRef](#)]
38. Voorwaldb, H.J.C.; Souzaa, R.C.; Pigatinc, W.L.; Cioffi, M.O.H. Evaluation of WC–17Co and WC–10Co–4Cr thermal spray coatings by HVOF on the fatigue and corrosion strength of AISI 4340 steel. *Surf. Coat. Technol.* **2005**, *190*, 155–164. [[CrossRef](#)]
39. De Medeiros Castro, R.; De Cesaro Cavaler, L.C.; Kejelin, N.Z.; Comeli, F.W.; Rocha, A.D.S. Revestimento WC depositado por aspersão térmica (HVOF) como alternativa ao cromo duro eletrodepositado aplicados em equipamentos hidráulicos. *Rev. Iberoam. Ing. Mec.* **2015**, *19*, 27–42.
40. Dent, A.H.; DePalo, S.; Sampath, S. Examination of the wear properties of HVOF sprayed nanostructured and conventional WC-Co cermets with different binder phase contents. *J. Thermal Spray Technol.* **2002**, *11*, 551–558. [[CrossRef](#)]
41. Holmberg, K.; Matthews, A. Coating Tribology: Properties, Mechanisms, Techniques and Applications in Surface Engineering. In *Tribology and Interface Engineering*; Elsevier: Amsterdam, The Netherlands, 2009.
42. Ma, N.; Guo, L.; Cheng, Z.; Wu, H.; Ye, F.; Zhang, K. Improvement on mechanical properties and wear resistance of HVOF sprayed WC-12Co coatings by optimizing feedstock structure. *Appl. Surf. Sci.* **2014**, *320*, 364–371. [[CrossRef](#)]
43. Laukkanen, A.; Holmberg, K.; Koskinen, J.; Ronkainen, H.; Wallin, K.; Varjus, S. Tribological contact analysis of a rigid ball sliding on a hard coated surface, Part III: Fracture toughness calculation and influence of residual stresses. *Surf. Coat. Technol.* **2006**, *200*, 3824–3844. [[CrossRef](#)]
44. Available online: <https://plasmascience.kz/ru/nczp/oborudovaniya> (accessed on 20 January 2022).
45. Topoliansky, P.A. *HVOF Termika-3 High-Speed Spraying Unit*; Technical Description and Operating Instructions: St. Petersburg, Russia, 2021. (In Russian)
46. Fauchais, P.L.; Heberlein, J.V.R.; Boulos, M.I. *Thermal Spray Fundamentals, From Powder to Part*; Springer: Berlin, Germany, 2014.
47. Agu, A.; Camo, F.; Garcí a de Blas, J.; del Hoyo, J.C.; Muelas, R.; Santaballa, A.; Ulargui, S.; Valle, P. HVOF-Deposited WCCoCr as Replacement for Hard Cr in Landing Gear Actuators. *J. Thermal Spray Technol.* **2011**, *20*, 1292–1309. [[CrossRef](#)]
48. Wang, Q.; Zhong, Y.; Li, H.; Wang, S.; Liu, J.; Wang, Y.; Ramachandran, C.S. Effect of Cobalt and Chromium Content on Microstructure and Properties of WC-Co-Cr Coatings Prepared by High-Velocity Oxy-Fuel Spraying. *Materials* **2023**, *16*, 7003. [[CrossRef](#)]
49. Magnania, M.; Suegamaa, P.H.; Reccob, A.A.C.; Guilemanyc, J.M.; Fugivaraa, C.S.; Benedettia, A.V. WC-CoCr coatings sprayed by high velocity oxygen-fuel (HVOF) flame on AA7050 aluminum alloy: Electrochemical behavior in 3.5% NaCl solution. *Mater. Res.* **2007**, *10*, 377–385. [[CrossRef](#)]
50. Kurlov, A.S.; Gusev, A.I. Phase equilibria in the system W-C and tungsten carbides. *Adv. Chem.* **2006**, *75*, 617. (In Russian) [[CrossRef](#)]
51. Wang, Q.; Tang, Z.; Cha, L. Cavitation and Sand Slurry Erosion Resistances of WC-10Co-4Cr Coatings. *J. Mater. Eng. Perform.* **2015**, *24*, 1–9. [[CrossRef](#)]
52. Liu, J.; Chen, T.; Yuan, C.; Bai, X. Performance Analysis of Cavitation Erosion Resistance and Corrosion Behavior of HVOF-Sprayed WC-10Co-4Cr, WC-12Co, and Cr₃C₂-NiCr Coatings. *J. Therm. Spray Tech.* **2020**, *29*, 798–810. [[CrossRef](#)]
53. Wang, Q.; Zhang, S.-Y.; Cheng, Y.-L.; Xiang, J.; Zhao, X.-Q.; Yang, G.-B. Wear and corrosion performance of WC-10Co4Cr coatings deposited by different HVOF and HVOF spraying processes. *Surf. Coat. Technol.* **2013**, *218*, 127–136. [[CrossRef](#)]
54. Picas, J.A.; Punset, M.; Baile, M.T.; Martín, E.; Forn, A. Effect of oxygen/fuel ratio on the in-flight particle parameters and properties of HVOF WC-CoCr coatings. *Surf. Coat. Technol.* **2011**, *205*, S364–S368. [[CrossRef](#)]
55. Chen, X.; Li, C.-D.; Gao, Q.-Q.; Duan, X.-X.; Liu, H. Comparison of Microstructure, Microhardness, Fracture Toughness, and Abrasive Wear of WC-17Co Coatings Formed in Various Spraying Ways. *Coatings* **2022**, *12*, 814. [[CrossRef](#)]
56. Pisarenki, G.S.; Borisenko, V.A.; Kashtalyan, Y.A. Effect of Temperature on the Hardness and Modulus of Elasticity of Tungsten and Molybdenum in the Temperature Range of 20 to 2700 C, Sov. *Powder Metall. Met. Ceram.* **1962**, *5*, 371–372. (In Russian)

Disclaimer/Publisher’s Note: The statements, opinions and data contained in all publications are solely those of the individual author(s) and contributor(s) and not of MDPI and/or the editor(s). MDPI and/or the editor(s) disclaim responsibility for any injury to people or property resulting from any ideas, methods, instructions or products referred to in the content.